Detecting 3D Corpus Callosum abnormalities in phenylketonuria

Qing He

Department of Computer Science,
University of Missouri, 65211, USA
E-mail: qhgb2@mizzou.edu

Shawn E. Christ

Department of Psychological Sciences,
University of Missouri, 65211, USA
E-mail: christse@missouri.edu

Kevin Karsch

Department of Computer Science,
University of Illinois, 61801, USA
E-mail: Karsch1@uiuc.edu

Amanda J. Moffitt

Department of Psychological Sciences,
University of Missouri, 65211, USA
E-mail: moffitta@missouri.edu

Dawn Peck

Department of Child Health,
University of Missouri, 65211, USA
E-mail: PeckDA@missouri.edu

Ye Duan

Department of Computer Science,
University of Missouri, 65211, USA
E-mail: duanye@missouri.edu
*Corresponding author

Abstract: Phenylketonuria (PKU) is a genetic disorder characterised by an inability to metabolise phenylalanine. Several studies have reported that the Corpus Callosum (CC) is one of the most severely affected structures with respect to volume loss in early treated PKU patients. In this work, we aim to detect the abnormalities of the CC in PKU from both global and local perspectives. 3D models of the CC are extracted from MRI data using a

semiautomatic segmentation method. In the global analysis, raw and scaled volumes of the CC are compared between PKU patients and the controls. An oriented bounding box of the CC is constructed and its length, width and height are used as the MRI traits in our study. The raw and scaled values of these traits are compared between patients and controls. In the local analysis, shape differences at every surface point of the CC between PKU patients and the controls are computed using Hotelling T^2 two-sample metric followed by a permutation test. The height of the CC is found to be significantly shorter in the patients and significant shape abnormalities in the genu and splenium of the CC is also found in the patients.

Keywords: PKU; phenylketonuria; CC; corpus callosum; MRI; shape analysis.

Reference to this paper should be made as follows: He, Q., Christ, S.E., Karsch, K., Moffitt, A.J., Peck, D. and Duan, Y. (2009) 'Detecting 3D Corpus Callosum abnormalities in phenylketonuria', *Int. J. Computational Biology and Drug Design*, Vol. 2, No. 4, pp.289–301.

Biographical notes: Qing He is currently a PhD student of Computer Science in the Computer Graphics and Image Understanding Lab at University of Missouri. She received her BE Degree from Nanjing University of Science and Technology in 2004 and ME Degree from Shanghai Jiao Tong University in 2006.

Shawn E. Christ is the Director of the Clinical Neuropsychology Laboratory. He obtained his PhD in 2004 from Washington University in St. Louis with a specialisation in clinical pediatric neuropsychology. He later completed a 2-year postdoctoral fellowship in cognitive neuroscience at Washington University during which his training focused on the utilisation of functional magnetic resonance imaging technology in humans and the study of the neurocognitive processes involved in deception and lying. He is currently Assistant Professor in the Department of Psychological Sciences at the University of Missouri and an Adjunct Professor at the MU Thompson Center for Autism and Neurodevelopmental Disorders.

Kevin Karsch recently graduated from the University of Missouri with a Bachelor's Degree in Computer Science and Mathematics. He is now a student at the University of Illinois working towards a PhD in Computer Science.

Amanda J. Moffitt is currently a Graduate student in the clinical psychology PhD program at the University of Missouri.

Dawn Peck is a Genetic Counselor at University of Missouri. She received her BS Degree in Biology from University of Missouri in 1997 and her MS Degree in Genetic Counselling from Beaver College, Philadelphia in 2000.

Ye Duan is the Director of the Computer Graphics and Image Understanding Lab and an Associate Professor of Computer Science at University of Missouri. He received his BA Degree in Mathematics from Peking University in 1991 and his MS Degree in Mathematics from Utah State University in 1996. He received his MS and PhD Degree in Computer Science from the State University of New York at Stony Brook in 1998 and 2003. His research interests include computer graphics and visualisation, biomedical imaging and computer vision, geometric and physics-based modelling, virtual reality and human-computer interaction, computer animation and simulation.

1 Introduction

Phenylketonuria (PKU) is a metabolic disorder that results from a deficiency of phenylalanine hydroxylase, which leads to elevated levels of the amino acid phenylalanine (Phe) in the blood. It is an autosomal recessive disorder caused by mutations in the PAH gene. The clinical behaviour of the untreated state is characterised by mental retardation, macrocephaly, seizures, eczema, and other behaviour abnormalities (National Institutes of Health Consensus Development Panel, 2001), and the brain pathology includes reduced brain weight and hypo- and demyelination of cerebral white matter (Scriver et al., 1995). However, the heterogeneity in the mutations of PAH results in wide phenotypic heterogeneity, and the relationship between the clinical phenotype and the genotype is not always constant (National Institutes of Health Consensus Development Panel, 2001).

By the application of a Phe-restricted diet beginning in the first days of life, the phenotype of untreated PKU can be prevented. Due to the prevalence of Phe in foods, even under dietary restriction, individuals with PKU still have higher-than-normal levels of Phe in their systems. Many comparisons between early treated PKU patients and controls showed cognitive and behavioural deficits in the patients. MR imaging studies on early treated PKU patients have primarily shown the volume loss in white matter regions of the brain in the patients (Thompson et al., 1993; Phillips et al., 2001; Hasselbalch et al., 1996; Pfaendner et al., 2005; Hahnel, 2008), although grey matter changes in cortical layering, tissue mass (atrophy), and reduced dendritic arborisation have also been reported (Dyer et al., 1996; Dyer, 2000). Although volume is a phenotype based on quantitative assessment of brain structures, no shape information about the brain structure can be revealed. Assessing shape changes is important in understanding how the volume is changed, e.g., a scaling (rigid transformation) of the shape vs. a distortion (non-rigid transformation). Quantitative assessment of the shape morphology can provide additional phenotypes and thus help in understanding the relationship between genetic mutation and phenotype variation in PKU.

The Corpus Callosum is a large white matter bundle connecting the left and right hemisphere and is the main neural conduit for interhemispheric interaction. It has been reported to be one of the most severely affected structures with respect to volume loss in early treated PKU patients (Pfaendner et al., 2005; Hahnel, 2008). Studies have found that early treated PKU patients displayed a disruption in communication between hemispheres, caused by abnormal myelination of neurons that make up the CC (Gourovitch et al., 1994; Banich et al., 2000).

The aim of this study is to detect size and shape abnormalities of the CC in early treated PKU. Two types of analysis are conducted. The first type is MRI traits analysis. An MRI trait is a phenotypic trait (Shyu et al., 2007) of an organism on MR images. Under this definition, volume can be considered a trait which is most commonly used. Other MRI traits can also be defined in various ways. In our study, traditional volume analysis is performed. Besides, an oriented bounding box of the 3D CC model segmented from MR images is constructed. The MRI traits are defined as the length, width, height of the bounding box and all the pairwise ratios, and they are to be compared between PKU and control groups. The second type is local shape analysis, which compares 3D shapes of the CC at every surface location. Shape analysis has gained an increasing amount of interest from the neuroimaging community because it can precisely locate morphological changes in pathological structures, which cannot be reflected in volume or

other MRI traits. The two types are complementary to each other. The first type provides global information about the difference between pathological structures and normal ones, while the second type reveals the local difference at specific locations.

Due to limited sample data at the current phase, this study serves as a pilot for analysing abnormalities of a pathological brain structure and some preliminary results are shown. Other related brain structures can also be studied using similar methods.

2 Methods

2.1 Participants and data

Eight participants with PKU (4 males, 4 females) who were diagnosed at birth and maintained on a phenylalanine-restricted diet participated in the study and ranged in age from 11 to 27 years ($M = 16.80$, $SD = 4.92$). Eight individuals without PKU (4 males, 4 females) comprised an age-, education-, and gender-matched control group. The control group ranged in age from 12 to 27 years ($M = 17.19$, $SD = 5.05$). Individuals with psychiatric and/or medical history unrelated to PKU were excluded.

All MRI scans were obtained on a 1.5T Siemens Symphony scanner with a standard 8-channel head coil. A high-resolution three-dimensional T1-weighted sagittal scan was collected for purposes of structural analysis (MP-RAGE sequence: TR = 1920 ms, TE = 4 ms, flip angle = 8°, in-plane resolution = 1 × 1 mm, slice thickness = 1 mm, number of slices = 160).

2.2 3D modelling of the CC

The CC models were obtained using a 3D semi-automatic hybrid (region- and boundary-based) segmentation method that had been previously validated for accuracy and reproducibility (Karsch et al., 2009). To further increase the accuracy and validity of the results, we ensured that all segmentations were completed by the same trained individual using the aforementioned method. An implicit voxel representation (i.e., a 3D binary image) and an explicit mesh representation of the model were both obtained after the segmentation. Each model was a 3D mesh with 3000~4000 points. The segmented CC model can be seen in Figure 1.

Figure 1 Two views of a 3D CC model and its oriented bounding box (red line: the length; green line: height; blue line: width) (see online version for colours)

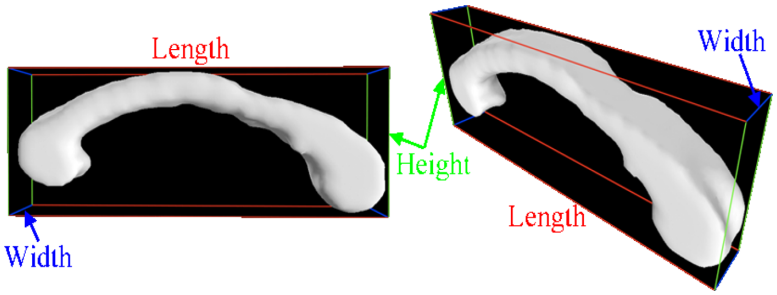

2.3 MRI traits measurements

We used the voxel representation for the volume analysis. The raw volume is the multiplication of the voxel count and the voxel size in mm^3. To take into account the effect of the brain volume, we normalise the raw CC volume by the Total Brain Volume (TBV) and the Intracranial Volume (ICV), respectively. TBV includes grey matter and white matter and excludes ventricles (Brien et al., 2006), and ICV is the sum of white matter, grey matter, and inner and outer cerebrospinal fluid spaces (Wolf et al., 2003). A choice can be made between using TBV or ICV as an adjustment factor (O'Brien et al., 2006), but our results show that the two choices do not make any difference. We used the FMRIB software library (Smith et al., 2004) for brain skull stripping, and then used a web-based program (Karsch et al., 2008) to calculate TBV and ICV. The brain volumes, raw and scaled volumes of the CC are compared between patients and controls.

We explored MRI traits based on the oriented bounding box of the CC model. Explicit representation of the model was used for this analysis. Principal Component Analysis (PCA) was used to find the principal orthogonal axes of the CC model, and the edges of the bounding box were parallel to one of these axes. Figure 1 shows two views of the CC model along with the bounding box. The length was defined as the frame which extended from the posterior to the anterior of the CC, the width was the frame that extended perpendicular to the sagittal plane, and the height was the other frame. We also calculated the ratio between each pair of orthogonal frames. The shape of the bounding box depends on both the size and the shape of the CC, so these MRI traits can reflect both size and shape information of the CC.

To account for the brain volume effect, we scaled the above raw measurements by the cubic root of TBV and ICV, respectively. Since these measurements were in mm, this scaling made the units consistent. Both raw and scaled measurements were compared between patients and controls.

2.4 Point correspondence establishment

Point correspondence among individual shapes is an essential and challenging procedure in local shape analysis. In our recent work (He et al., 2009) we developed a landmark sampling method to find point correspondence which was an improved version of Dalal et al. (2007). We briefly describe here how to find the correspondence between two 3D meshes, and the same method can be generalised to a group of shapes.

Given two triangle meshes U and V, we first removed the location difference by moving their centres of mass to the origin. Then we normalised each shape by its centroid size (Bookstein, 1989) so that there is no size effect in the following shape analysis. The rotation between the two shapes was removed by aligning their principle axes. After spatial alignment we constructed a set of landmarks on the template shape U. These landmarks need not be anatomically defined. The basic consideration is that they should be dense enough to represent the surface U and sufficiently sparse for a compact statistical shape model. The 3D space is divided into equal-sized cubic cells. In each cell, the surface point closest to the centre of the cell is selected as the landmark. The size of the cell controls the density of landmarks. A comparison of the original surface points and the sampled landmarks can be seen from Figure 2(a) and (c).

Figure 2 (a) Two aligned original point clouds overlaid (blue: template, red: target); (b) initial landmarks on the target shape obtained using the algorithm in Dalal et al. (2007) and (c) our algorithm (see online version for colours)

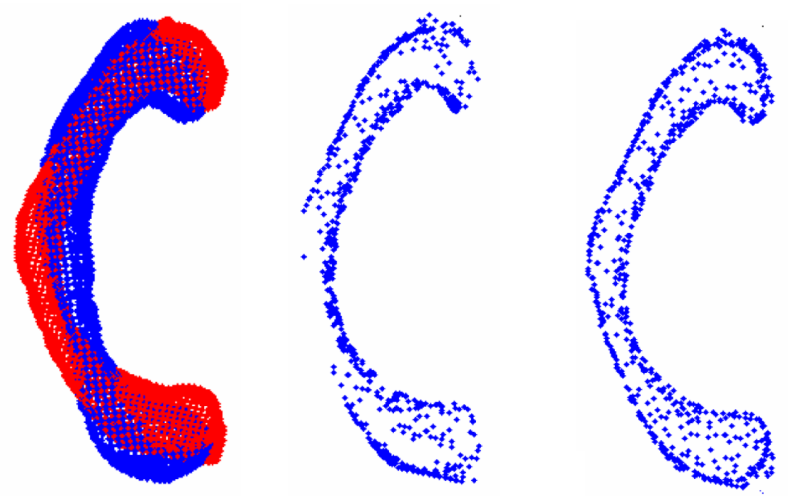

(a) (b) (c)

We then found the landmarks (a subset of surface points) on the target shape V that corresponded with the template landmarks. A simple way is to select a closest point on the target triangle mesh for each landmark on the template (Dalal et al., 2007). Since the two shapes are pre-aligned, it is assumed that this simple method can find a rough correspondence between the landmarks on U and V. However, if the two aligned shapes do not have a certain amount of overlapping (e.g., Figure 2(a)), this method may fail to find the correct correspondence. In order to solve this problem, we proposed an improved initial correspondence algorithm with a mutual selection strategy and normal constraints (He et al., 2009). We observed that if the two points are corresponding points on two shapes, their surface normal directions should not differ too much. If their surface normal directions are nearly opposite, they are not likely to be the corresponding points. We used the constraint of normal directions in addition to the distance in the landmark selection procedure. Let the set of template landmarks be U_L, each template landmark $u_i \in U_L$, the original point set on the target mesh be V, each target point $v_i \in V$, and the set of target landmarks be V_L. Our algorithm can be outlined as follows.

1 For each $v_j \in V$, find a landmark u_i from U_L which is closest to v_i.

2 For each $u_i \in U_L$, record all the v_j's that select u_i as the closest point. Denote this set of v_j's as V_i.

3 If u_i has more than one point in its V_i, find a point v_j from V_i whose normal direction is closest to the normal of u_i. Remove v_j from V and add it to V_L. If u_i has no points in its V_i, find a point v_j from V that has closest distance to u_i. Remove v_j from V and add it to V_L.

The resulting points in V_L are the corresponding landmarks on the target shape. Figure 2 shows a real example of the initial landmarks on the target CC shape obtained using the simple way and our algorithm, respectively.

Given the initial correspondence between two sets of landmarks, U_L and V_L, one can estimate a transformation T from V_L to U_L, and T can be applied to the entire target point set V. We now briefly introduce the basic concept of TPS. Suppose there are n landmarks in U_L and V_L, respectively. Let the landmarks in U_L be $u_i = (u_{ix}, u_{iy}, u_{iz})$, and the landmarks in V_L be $v_i = (v_{ix}, v_{iy}, v_{iz})$, $i = 1, \ldots, n$. u_i and v_i are corresponding points for the same i. The TPS function which transforms v_i to u_i has the form:

$$f(v_{ix}, v_{iy}, v_{iz}) = a_0 + a_x v_{ix} + a_y v_{iy} + a_z v_{iz} + \sum_{j=1}^{n} w_j \phi(\| (v_{jx}, v_{jy}, v_{jz}) - (v_{ix}, v_{iy}, v_{iz}) \|) \quad (1)$$

where $\phi(r) = r$ in 3D case. We use three separate functions to model the transformation of x, y, z coordinates, and the objective function is

$$T(v_{ix}, v_{iy}, v_{iz}) = (f_x(v_{ix}, v_{iy}, v_{iz}), f_y(v_{ix}, v_{iy}, v_{iz}), f_z(v_{ix}, v_{iy}, v_{iz})) = (u_{ix}, u_{iy}, u_{iz}). \quad (2)$$

Each function f_x, f_y, f_z has the same form as equation (1). Equation (2) can be written in the matrix form and the coefficients a_0, a_x, a_y, a_z, w_i of each function can be solved from the linear equation.

After we obtain the initial correspondence between U_L and V_L, we estimate a TPS transformation from V_L to U_L, and apply the transformation function to the entire point set V. The transformed target point set is denoted as V^1, and the algorithm in 2.2 is then applied on U_L and V^1 to find a set of target landmarks V_L^1. Then a TPS transformation from V_L^1 to U_L is estimated and applied to V^1. The final landmark set V_L^n after n iterations contains the landmarks in the transformed shape V^n. We keep track of the indices of the landmarks in each iteration, so that the final landmarks can be easily mapped to their original coordinates in V. After several iterations, the initial correspondence error can be greatly reduced. As suggested in Dyer et al. (1996), three iterations are used in our experiment. Figure 3 shows one example of landmarks before and after three TPS iterations.

Figure 3 The landmarks on a target shape before (left) and after (right) TPS iterations (see online version for colours)

2.5 *Statistical shape analysis*

One of the 16 meshes was randomly selected as the template, and 767 landmarks were sampled on this template. The correspondence between this template and each of the other shapes was established using our algorithm, and the result was 16 sets of corresponded landmarks, which can be used directly for statistical shape analysis.

Since each shape is spatially aligned with the template before the shape correspondence is established, no additional spatial alignment is necessary among all the shapes. The difference in the size of the CC has been eliminated in the spatial alignment, so the shape analysis only reveals pure shape difference between patients and controls. Hotelling T^2 two-sample metric is used to measure how two groups of shapes are different from each other at each surface location. We use a modified T^2 metric instead of the standard one, because it is less sensitive to group differences of the covariance matrixes and the sample size (Styner et al., 2006). This metric is defined as

$$T^2 = (\mu_1 - \mu_2)'((1/n_1)\Sigma_1 + (1/n_2)\,\Sigma_2))^{-1}\,(\mu_1 - \mu_2) \tag{3}$$

where Σ_1, Σ_2 are the covariance matrices of the two groups, μ_1, μ_2 are the average coordinates of the two groups at this surface point, and n_1, n_2 are the sample sizes of the two groups. A positive, larger T^2 indicates more significant group difference, and each T^2 is converted to a corresponding p-value at every surface location. This raw p-value is an optimistic estimation. Since comparisons are made at thousands of CC surface points, it is important to control for the multiple testing problem. In our work, we adopt False Discovery Rate (FDR) (Hochberg and Benjamini, 1995) as the appropriate approach for p-value correction, because it provides an interpretable and adaptive criterion, while non-parametric permutation tests are overly pessimistic (Styner et al., 2006). FDR method allows the false positive to be within a small proportion α ($\alpha = 0.01$ in our experiment). The p-value correction is computed as follows.

1 Sort the p-values such that $p_1 < p_2 < \cdots < p_N$, where N is the number of vertices on the surface.

2 From all the p-values that satisfy $p_i <= \alpha \bullet i/N$, select the p-value with the largest index i, denoted as p_α.

3 Declare all locations with p-values less than p_α significant.

3 Results

3.1 MRI traits analysis

Two-tailed t-tests and two-tailed Mann-Whitney-Wilcoxon (MWW) (Conover, 1980) tests were used for statistical comparison of the MRI traits. The MWW test is similar to t-test and primarily suited for smaller data sets such as ours. A significance level of 0.05 was selected for both tests. Table 1 shows the results of the two tests in each comparison.

The two testing methods showed similar results. No significant difference was found between the two groups in the brain volumes, raw CC volumes and scaled CC volumes. Both tests indicated significant difference in the height of the bounding box of the CC. Both raw and scaled values of the height were significantly shorter in PKU patients than in the controls.

Table 1 Results of the CC analysis comparing patients with PKU to control data. Bold entries indicate a significant difference between the patients and the controls

Measurements	*Patients*		*Controls*		*t statistic*	*p-value*	*U statistic*
	Mean	*Std*	*Mean*	*Std*			
TBV ($\times 10^4$ mm^3)	128	8.68	126	7.73	0.2891	0.7767	29
ICV ($\times 10^4$ mm^3)	147	11.7	142	13.2	0.7884	0.4436	26
CC volume ($\times 10^4$ mm^3)	54.2	0.0636	55.3	0.0631	–0.3314	0.7453	31
CC volume/TBV($\times 10^{-3}$)	4.3	0.535	4.4	0.638	–0.4426	0.6648	30
CC volume/ICV ($\times 10^{-3}$)	3.7	0.461	3.9	0.781	–0.7490	0.4663	30
CC length (mm)	71.9	4.47	76.2	6.18	–1.5712	0.1385	21
CC height (mm)	26.9	5.68	33.0	5.43	–2.1848	**0.0464**	**12**
CC width (mm)	10.4	1.28	11.0	2.48	–0.6789	0.5083	30
CC length/ CC height	2.78	0.619	2.35	0.219	1.7958	0.0941	15
CC length/ CC width	7.03	0.889	7.19	1.58	–0.2513	0.8053	40
CC height/ CC width	2.63	0.633	3.13	0.903	–1.2727	0.2238	22
CC length/(TBV)$^{1/3}$	0.664	0.0399	0.706	0.0693	–1.4926	0.1577	24
CC height/(TBV)$^{1/3}$	0.247	0.0492	0.306	0.0550	–2.2294	**0.0427**	**12**
CC width/(TBV)$^{1/3}$	0.956	0.0127	0.102	0.0216	–0.6977	0.4968	28
CC length/(ICV)$^{1/3}$	0.633	0.0362	0.680	0.0729	–1.6268	0.1261	24
CC height/(ICV)$^{1/3}$	0.236	0.0470	0.295	0.0566	–2.2547	**0.0407**	**11**
CC width/(ICV)$^{1/3}$	0.912	0.0120	0.0979	0.0203	–0.8032	0.4353	28

3.2 *Local shape analysis*

Figure 4 gives a descriptive visualisation of the group shape difference. Figure 4(a) shows the overlaid average shape of each group, and Figure 4(b) shows the signed distance map between the two average shapes rendered on an overall average shape of all 16 subjects. By examining the average structures, we find that in the patients in whom the body of the CC is less bent, the anterior tip (genu) and posterior tip (splenium) are shorter, and the anterior most is more projected. Note that the triangle mesh information is lost after landmark sampling, and we reconstruct the surface using COCONE (Dey and Giesen, 2001) for display purpose.

Figure 4 (a) Two views of the overlaid average shapes (blue: controls, red: patients) and (b) two views of the distance map between the two average shapes. The negative distances (shown in blue) indicate the patients' structure is inside the controls' and the reverse (shown in red) is for the positive distances) (see online version for colours)

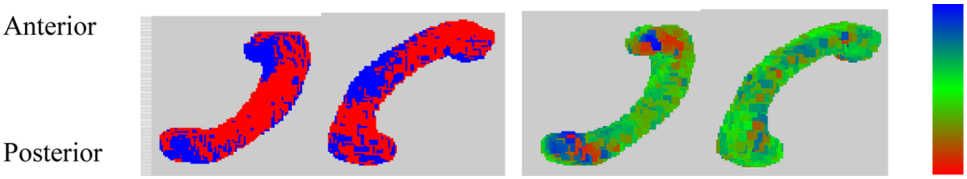

(a) (b)

The significance maps of the raw and corrected *p*-values are shown in Figure 5. Smaller *p*-values indicate larger statistical significance. A two-tailed alpha level of 0.05 is chosen as the significance threshold for the raw *p*-values, and FDR threshold p_α is 0.01 for corrected *p*-values. Figure 5(a) shows the significance map of raw *p*-values, which is an optimistic estimation. The significance map of the corrected *p*-values (Figure 5(b)) shows that the major significant difference lies in the genu and splenium. This is consistent with the distance map in Figure 4(b) which shows the main difference between the averages at these parts.

Figure 5 Significance map: (a) raw *p* values and (b) corrected *p* values (see online version for colours)

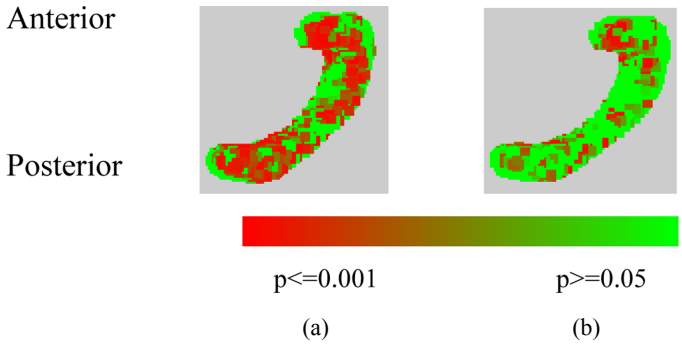

4 Conclusion and discussion

This study investigated the abnormalities of the CC in PKU patients through MRI traits analysis and local shape analysis. Volumes and bounding box based MRI traits of the CC were measured and scaled by TBV and ICV. Both raw and scaled measurements were compared between patients and controls using *t*-tests and MWW tests. Shape comparison is conducted at each surface location using the Hotelling T^2 test, followed by a permutation test. MRI traits analysis gives global information of the abnormalities, while shape analysis detects local surface morphology of the structure.

Most previous studies reported white matter loss in early treated PKU patients, and the CC is one of the most severely affected structures. These volumetric findings may help to determine whether patients with PKU should be recommended to receive lifelong dietary treatment or not. However, we did not find any significant difference in the raw and scaled CC volumes between PKU and controls. This might be due to our small sample size or the heterogeneity of PKU population. Interestingly, we did find significant reduction in both raw and scaled CC height in PKU patients, which has not been reported in any previous studies. Further more, we find significant shape abnormalities in the genu and splenium of the CC in PKU patients. This local shape morphology cannot be detected using global analysis such as MRI traits analysis, and it also has not been reported before. This might serve as additional evidence for the association with abnormal myelination of neurons that make up the CC. It is suggested that the relationship between variations in the phenotypes associated with blood Phe concentration be studied (National Institutes of Health Consensus Development Panel, 2001). Correlation between volumes of brain structures and blood Phe value has been studied and no significant correlation was found

(Pfaendner et al., 2005; Hahnel, 2008). Our MRI traits can serve as additional phenotypes to the volume, and their relation with blood Phe value can be studied in a similar manner. This will provide stronger evidence of whether or not patients with PKU should receive lifelong dietary treatment.

The clinical results of this study need to be interpreted cautiously due to the limitation of the sample size. The sample size is small compared with other statistical analysis, so the results may not be representative enough for large population. Since previous brain MRI studies revealed only volume loss of the CC in PKU patients and few have conducted local shape analysis or other MRI traits analysis of the CC, we cannot compare our results with other works. Therefore, this study serves as a pilot study about the shape morphology of the CC in early treated PKU and further study with larger sample sizes is needed to confirm the results.

In conclusion, we found no significant volume difference in the CC between early treated PKU patients and the controls, but we did find reduced CC height and significant shape abnormalities in the genu and splenium of the CC in PKU patients. This may provide phenotypic variation in addition to volume changes which can be associated with blood Phe level and other metabolic parameters.

Acknowledgements

The work reported here was supported by grant from the MU Thompson Center for Autism and Neurodevelopmental Disorders (SEC). Qing He is supported in part by a NIH clinical bio-detective predoctoral fellowship. Ye Duan is supported in part by the DoD autism concept award and the NARSAD Foundation young investigator award. We would like to thank Julie Grasela for her assistance with participant recruitment and Deanna Barch, Todd Braver, and Desirée White for their assistance with technical issues related to data collection.

Financial disclosures

Dr. Christ and Mrs. Peck serve as consultants for BioMarin Pharmaceutical Inc. No authors reported any biomedical financial interests or potential conflicts of interest.

References

Banich, M.T., Passarotti, A.M., White, D.A., Nortz, M.J. and Steiner, R.D. (2000), 'Interhemispheric interaction during childhood: II. Children with early-treated phenylketonuria', *Dev. Neuropsychol.*, Vol. 18, No. 1, pp.53–71.

Bookstein, F. (1989) 'Principal warps: thin-plate splines and the decomposition of deformations', *IEEE Transactions on Pattern Analysis and Machine Intelligence*, Vol. 11, No. 6, pp.567–585.

Conover, W.J. (1980) *Practical Nonparametric Statistics*, 2nd ed., John Wiley & Sons, pp.225, 226.

Dalal, P., Munsell, B.C., Wang, S., Tang, J., Kenton, O., Ninomiya, H., Zhou, X. and Fujita, H. (2007) 'A fast 3D correspondence method for statistical shape modeling', *IEEE Conference on Computer Vision and Pattern Recognition*, Minneapolis, MN.

Dey, T. and Giesen, J. (2001) 'Detecting undersampling in surface reconstruction', *Proc. 17th ACM Sympos. Comput. Geom.*, pp.257–263.

Dyer, C.A. (2000) 'Comments on the neuropathology of phenylketonuria', *Eur. J. Pediatr.*, Vol. 159, Suppl. 2, pp.S107–S108.

Dyer, C.A., Kendler, A., Philibotte, T., Gardiner, P., Cruz, J. and Levy, H.L. (1996) 'Evidence for central nervous system glial cell plasticity in phenylketonuria', *J. Neuropathol Exp. Neurol.*, Vol. 55, pp.795–814.

Gourovitch, M.L., Craft, S., Dowton, S.B., Ambrose, P. and Sparta, S. (1994) 'Interhemispheric transfer in children with early-treated phenylketonuria', *J. Clin. Exp. Neuropsychol.*, Vol. 16, No. 3, June, pp.393–404.

Hahnel, S. (2008) 'Brain MRI abnormalities in Phenylketonuria', *Clinical Neuroradiology*, Vol. 18, pp.19–24.

Hasselbalch, S., Knudsen, G.M., Toft, P.B., Hogh, P., Tedeschi, E., Holm, S., Videbaek, C., Henriksen, O., Lou, H.C. and Paulson, O.B. (1996) 'Cerebral glucose metabolism is decreased in white matter changes in patients with phenylketonuria', *Pediatr. Res.*, Vol. 40, pp.21–24.

He Q., Duan Y., Karsch K. and Miles J.H. (2009) 'Detecting corpus callosum abnormalities in essential autism based on anatomical landmarks', *Psychiatry Research: Neuroimaging*, under review.

Hochberg, Y. and Benjamini, Y. (1995) 'Controlling false discovery rate: a practical and powerful approach to multiple testing', *Journal of the Royal Statistical Society*: *Series B*, No. 57, pp.289–300.

Karsch, K., Grinstead, B., He, Q. and Duan, Y. (2008) 'Web based brain volume calculation for magnetic resonance images', *30th Annual International Conference of the IEEE Engineering in Medicine and Biology Society*, 20–24 August, Vancouver, BC, Canada.

Karsch, K., He, Q. and Duan, Y. (2009) 'A fast, semi-automatic brain structure segmentation algorithm for magnetic resonance imaging', *IEEE International Conference on Bioinformatics and Biomedicine*, 1–4 November, Washington DC, USA, Accepted.

National Institutes of Health Consensus Development Panel (2001) 'National institutes of health consensus development conference statement: phenylketonuria: screening and management 2000', *Pediatrics*, Vol. 108, 16–18 October, pp.972–982.

O'Brien, L.M., Ziegler, D.A., Deutsch, C.K., Kennedy, D.N., Goldstein, J.M., Seidman, L.J., Hodge, S., Makris, N., Caviness, V., Frazier, J.A. and Herbert, M.R. (2006) 'Adjustment for whole brain and cranial size in volumetric brain studies: a review of common adjustment factors and statistical methods', *Harvard Review of Psychiatry*, Vol. 14, No. 3, pp.141–151.

Pfaendner, N.H., Reuner, G., Pietz, J., Jost, G., Rating, D., Magnotta, V.A., Mohr, A., Kress, B., Sartor, K. and Hahnel, S. (2005) 'MR imaging-based volumetry in patients with early-treated phenylketonuria', *American Journal of Neuroradiology*, Vol. 26, No. 7, pp.1681–1685.

Phillips, M.D., McGraw, P., Lowe, M.J., Mathews, V.P. and Hainline, B.E. (2001) 'Diffusion-weighted imaging of white matter abnormalities in patients with phenylketonuria', *Am. J. Neuroradiol.*, Vol. 22, pp.1583–1586.

Scriver, C.R., Kaufman, S., Eisensmith, R.C. and Woo, S.L.C. (1995) 'The hyperphenylaninemias', in Scriver, C.R., Beaudet, A.L., Sly, W.S. and Valle, D. (Eds.): *Metabolic Basis of Inherited Disease*, 17th ed., McGraw-Hill, Vol. 1, New York, NY, pp.1015–1107.

Shyu, C., Green, J.M., Lun, D.P.K., Kazic, T., Schaeffer, M. and Coe, E. (2007) 'Image analysis for mapping immeasurable phenotypes in maize', *IEEE Signal Processing Magazine*, pp.115–118.

Smith, S.M., Jenkinson, M., Woolrich, M.W., Beckmann, C.F., Behrens, T.E.J., Johansen-Berg, H., Bannister, P.R., De Luca, M., Drobnjak, I., Flitney, D.E., Niazy, R., Saunders, J., Vickers, J., Zhang, Y., De Stefano, N., Brady, J.M. and Matthews, P.M. (2004) 'Advances in functional and structural MR image analysis and implementation as FSL', *NeuroImage*, Vol. 23, No. S1, pp.208–219.

Styner, M., Oguz, L., Xu, S., Brechbuehler, C., Pantazis, D., Levitt, J.J., Shenton, M.E. and Gerig, G. (2006) 'Framework for the statistical shape analysis of brain structures using SPHARM-PDM', *The Insight Journal – 2006 MICCAI Open Science Workshop*, available at http://hdl.handle.net/1926/215

Thompson, A.J., Tillotson, S., Smith, I., Kendall, B., Moore, S.G. and Brenton, D.P. (1993) 'Brain MRI changes in Phenylketonuria: associations with dietary status', *Brain*, Vol. 116, pp.811–821.

Wolf, H., Kruggel, F., Hensel, A., Wahlund, L., Arendt, T. and Gertz, H. (2003) 'The relationship between head size and intracranial volume in elderly subjects', *Brain Research*, Vol. 972, No. 1, pp.74–80.